A 2D Lattice Boltzmann Full Analysis of MHD Convective Heat Transfer in Saturated Porous Square Enclosure

Ridha Djebali[1,2]**, Mohamed ElGanaoui**[3] **and Taoufik Naffouti**[1]

Abstract: A thermal lattice Boltzmann model for incompressible flow is developed and extended to investigate the natural convection flow in porous media under the effect of uniform magnetic field. The study shows that the flow behaviour is various parameters dependent. The Rayleigh number (Ra), Hartmann number (Ha), Darcy number (Da) and the medium inclination angle from the horizontal (ϕ), the magnetic field orientation (ψ) and the medium porosity (ε) effects are carried out in wide ranges encountered in industrial and engineering applications. It was found that the flow and temperature patterns change significantly when varying these parameters. To confirm the accuracy in present simulations, the present results are first validated on two test cases with and without magnetic field. A good agreement is observed by comparison with available previous works. It is found also that the lattice Boltzmann method is a reliable tool that gives a great deal of valuable information about the dynamics of buoyancy-driven flows and put on view the physics of the flow under stiff conditions.

Keywords: Lattice Boltzmann computer modeling, magnetic fluid, heat transfer, porous media flow, thermal convection.

Nomenclature

B	Magnetic field
$\overline{Nu}$	Average overall Nusselt number
$\mathbf{e}_k$	Discrete lattice velocity
$\overline{Nu}_0$	Nusselt number at the hot wall
F	Total external forcing term

[1] Univ. de Tunis El Manar, Faculté des Sciences de Tunis / LETTM,2092 Manar II, Tunis. ridha.djebali@ipein.rnu.tn

[2] CNRS-SPCTS / CEC 12, Rue Atlantis 87068, Limoges, France.

[3] Univ. de Lorraine, IUT Henri Poincaré / LERMAB-Longwy, 186-Rue de Lorraine, 54400 Cosnes et Romain, France

g	Gravity field
u	Velocity vector (u, v)
x	Lattice node in (x, y) coordinates
c_s	Lattice sound speed
f_k, g_k	Discrete distribution functions.
H	Height of the enclosure
k_e	Effective thermal conductivity
p	Ideal gas pressure ρc_s^2
S_k	Source term
T	Temperature field
ΔT	Horizontal temperature gradient $T_h - T_c$
Δt	Time step
Δx	Lattice spacing units $(= \Delta y)$
F_ε	Geometric parameter
Da	Darcy number
Ha	Hartmann number
Pr	Prandtl number υ / α
Ra	$g\beta \Delta T H^3 / \nu \alpha$ Rayleigh number

Greek symbols

w_k	Weighting factors
ρ	Fluid density (volumetric mass)
υ	Kinetic viscosity $= \mu / \rho$
α	Thermal diffusivity $k_e / (\rho C_p)_f$.
$\tau_\upsilon, \tau_\alpha$	Relaxation times for f_k and g_k
ε	Medium porosity
β	Thermal expansion coefficient
ϕ	Angle of inclination of the cavity
ψ	Magnetic field inclination angle
η	Structural factor
Λ	Effective averaged heat capacity
κ	Medium permeability

Subscripts Supscripts

| eq | Equilibrium part |
| i, j | Lattice vector components |

k	Discrete velocity direction
LD,NLD	Linear and non-linear drags
new, old	Time-successive states

1 Introduction

Natural convection in enclosures depends strongly on many parameters monitoring the flow behaviour in specila industrial situations, namely the Rayleigh and the Prandtl number and the medium inclination angle and its configuration. Moreover, flows in medium packed with porous materials are frequently encountered in many practical applications in fluid mechanic and engineering such as solar power collectors, chemical catalytic reactors, heat exchangers, building thermal insulation, nuclear energy, petroleum reservoir operations, packed-bed catalytic reactors, food processing and so on...

In general, transport phenomena in porous medium involve three scales: the pore scale, the representative elementary volume (REV) scale and the domain scale. The first approach needs much detailed geometric details to reach the local information of the fluid flow. The computational domain size will, however, not be permitted due to the limited computer resources. The REV scale approach is considered as the minimum size scale to determine statistically the macroscopic quantities and is the most adopted in the previous porous media flows studies. This approach, based on some semi-empirical models, is incorporated in the evolution equations by adding forcing term taking account of the porous medium characteristics. These semi-empirical models are based on the Ergun's experimental investigations to express some geometric parameters linked to the porous medium porosity.

In the literature, numerous models have been used to simulate flows in porous media, such as the Darcy model, the Brinkman-extended Darcy model, and the Forchheimer-extended Darcy model. The Darcy model (1856) scheme is an empirical law; where the pressure gradient is related to the viscous resistance based on experimental observations.

Although the Darcy model has been widely used to investigate flow in porous media, it was limited to low infiltration velocities. For high velocities, the so-called non-Darcy effects (viscous dissipation due to the solid boundary in the porous matrix and the inertia) are to be considered. The Brinkmann-extended-Darcy model (1947) was developed for accounting for viscous force. However, this model does not show agreement with experimental observations only for high porosity ($\varepsilon \rightarrow 1$), also it presents difficulty to evaluate the equivalent viscosity of the medium that is function of both the porosity and the tortuous character of the medium. The

Forchheimer-extended Darcy (1901) model was improved by Vafai and Tien (1981) using a local volume averaging technique to account for the inertia effect. It is currently the most widely used to simulate incompressible steady fluid flows through saturated homogenous and isotropic porous medium. The three mentioned models are, also, not generalized to be applicable for a medium with a variable porosity.

In spite of the several experimental efforts and the numerical simulations based on the semi-empirical models (Amahmid, Hasnaoui et al. (1999); Jiang and Ren (2001); Anwar- Hossain, Wilson (2002); Basak, Roy, et al. (2006); Srivastava and Singh (2010); Hamimid et al. (2011)), flows in porous medium remain of particulars interest and the basic picture stays clouded. In recent years, a new *generalized model* has been adopted by researchers interested by modeling these type-?ows (Nithiarasu, Seetharamu et al. (1997)). The generalized model form is a modified formulation of the Navier-Stokes equations, involving all the fluid forces and the solid matrix drag in the momentum equations. In general, the generalized model presents three pertinent features. First, its similarity to the Navier-Stokes equations allows the transitions to free fluid flow (when the porosity be the unit); second, it presents the flexibility to represent the two extended models (Brinkman-extended Darcy and Forchheimer-extended Darcy models), which are regarded as its limiting forms; and third, this model can be used to solve transient flows in porous media.

A large number of studies have confirmed the earlier developments. Besides, recent books by Nield and Bejan (2006), Ingham and Pop (2005), Vafai (2005) and Pop and Ingham(2001) show that investigating flows in porous medium becomes a classical subject. Furthermore, flows under external magnetic field are of practical interest and have been the subject of many earlier and recent studies for free fluid flows (Gelfgat and Bar-Yosaf (2001), Ece and Büyük (2006)). However, few studies have been conducted to fully investigate the heat transfer in porous medium with/ without the effect of external magnetic field (Grosan, Revnic et al. (2009)) under the numerous controlling parameters.

Furthermore, the study of the motion and heat transfer in electrically conducting fluid has met always with renewed interest due to the many applications in engineering problems such as MHD generators, plasma studies, nuclear reactors, and because of the effect on magnetic fields on the performance of many systems including liquid metals and alloys, mercury amalgams, and blood...

Several numerical simulations have been conducted in the past using conventional numerical method based on discretization of macroscopic equations. Recently, the Lattice Boltzmann Method (LBM) has met with significant success for numerical simulation and modeling of many classical and complex flows (Chen and Doolen (1998), Mezrhab, Jami et al. (2007), Semma, El Ganaoui et al. (2008), Succi

(2001)). The LBM have been used recently to investigate flows in porous media. For citation, Guo and Zhao (2002) use the LB method to investigate Poiseuille flow, Couette flow and lid-driven cavity flow in a saturated porous media, authors used a suitable forcing term early improved by Guo, Zheng et al. (2002) to eliminate the discrete lattice effects in the forcing term used in the LB equation. The developed model is useful in simulating flows in a medium with a variable porosity. It has been observed that the developed model produces satisfactory results for the above cited problems compared with the analytical or the finite-difference solutions. Seta, Takegoshi et al. (2006) used the same approach to investigate flow in porous media in square enclosure. It has been concluded that the LB method preserves more the computational cost than the FD method for the same grid size and gives a good agreement compared to the FE method either for the Brinkman-extended Darcy model and the Brinkman–Forchheimer model. Arab, Semma, Pateyron and El-Ganaoui (2009) used a LB based numerical code to read (after special treatment) 2D digital images obtained by a Scanning Electron Microscope technique. The authors concluded on the LB method high level of predictability of heat and mass transfer phenomena in real porous material and to estimate physical properties such as the medium permeability which is hardly estimated experimentally. Chai, Guo et al. (2007) have investigated mixed heat convection in a driven cavity packed with porous media. Authors concluded that compared with traditional numerical methods, LBM offers flexibility, efficiency and outstanding amenability to parallelism when modeling complex flows.

Besides, Roussellet, Niu et al. (2011) used the LB method to investigate heat and fluid flow in a cubical porous medium packed with a set number of balls under a temperature sensitive magnetic field. It was found that heat transfer is enhanced by increasing the magnetic field; however it is reduced by increasing the balls number. Hao, Xinhua and Yongzhi (2011) simulated a multi-component system formed by fluid and magnetic particles using a multiphase LB model, under external magnetic field. Authors concluded that the LB method is so helpful to explore and understand the chainlike particles behavior when applying external magnetic field on a random distribution of particles. Chatterjee and Amiroudine (2011) used a non-isothermal LB model to predict the thermofluidic phenomena in a direct current MHD microp-ump. It was remarked that flow and heat transfer characteristics depend strongly on Hartmann, Prandtl and Eckert numbers and channel aspect ratios. An excellent agreement is also observed between LB results and experimental, analytical and other available numerical results in the literature. Ece and Büyük (2006) have investigated the steady laminar natural-convection flow in an inclined square enclosure heated and cooled from adjacent sides in the presence of a magnetic field. The governing equations based on the stream function, vorticity and temperature

have been solved using the differential quadrature method for various Grashof and Hartman numbers and aspect ratios, inclination of the cavity and magnetic field orientations. Its has been observed that the flow characteristics, therefore the heat transfer rate are affected significantly by the variation of Hartman number, the aspect ratio and the inclination of the enclosure. Zhang, Jin et al. (2010) introduced a LB model to investigate a thermo-sensitive magnetic fluid in porous medium. Authors obtained excellent agreement with previous results and concluded that the LB method is a promising tool for understanding magnetic fluid non-isothermal behaviour in porous media.

Through this literature review, one can remark that the flow patterns and isotherms exhibit *distinctly* different behavior in differentially heated enclosures by varying each monitoring parameter. Additionally, no / very little works has been reported on this topic with full assessment of *all* flow parameters effects, and no focus is made on the *computational cost* in general when treating some heat transfer problem.

In the present paper, a thermal lattice Boltzmann model is developed and used to investigate the dynamic and thermal behavior in porous medium under inclined uniform magnetic field in a square enclosure. The effects of the Rayleigh number, the cavity inclination, the magnetic field magnitude (Hartmann number) and its orientation and the porous matrix effects (Darcy number and the medium porosity) -in wide ranges- on flow and heat transfer are analyzed and tabulated for benchmarking purposes. A simple and efficient accelerating technique is used to improve the convergence process.

2 Problem Statement and Solution Method

2.1 Configuration Model and Parameterization

The investigated problem is a two-dimensional square enclosure of edge H packed with a saturated porous media. The porous material is supposed to be homogeneous and isotropic with constant porosity. The non-slip boundary conditions hold on the four walls. A temperature difference $\Delta T = T_h - T_c$ is applied between walls parallel to y-direction ($T = T_h$ for $x = 0$ and $T = T_c$ for $x = H$) and zero heat flux is imposed to walls parallel to x-direction. The cavity is clockwise inclined by an angle ϕ. A magnetic field of strength B reigns in the medium. The magnetic field is oriented to angle ψ from x-axis (Fig. 1). The gravity field reigns in the vertical descendant direction.

For the sake of comparison with previous studies, all predicted quantities are presented in a non-dimensional form. The reference scales $l_0 = H$, $U_0 = \alpha/H$ $t_0 = H^2/\alpha$, $p_0 = \rho U_0^2$ and $\Delta T = T_h - T_c$ are used for length, velocity, time pressure and relative temperature respectively. Here α is the effective thermal diffusivity.
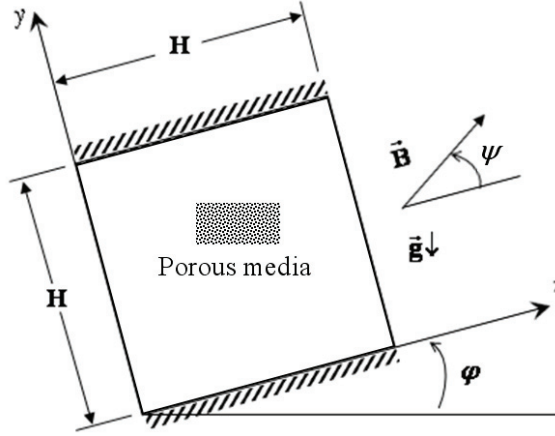
Figure 1: Configuration model

The convective heat transfer is described using the average Nusselt number $\overline{Nu}$ overall the whole domain and the average Nusselt number $\overline{Nu}_0$ along the hot wall

$$\overline{Nu} = \frac{1}{\alpha \Delta T / H} \frac{1}{H^2} \int_0^H \int_0^H [uT - \alpha (\partial T / \partial x)] \, dx \, dy \qquad (1)$$

$$\overline{Nu}_0 = \frac{1}{\alpha \Delta T / H} \frac{1}{H} \int_0^H -\alpha \left. \frac{\partial T}{\partial x} \right|_{x=0} dy \qquad (2)$$

The flow is characterized by the Rayleigh number ($10^4 \leq Ra \leq 10^7$), the Prandtl number ($\Pr \simeq 1$), the Darcy number ($10^{-4} \leq Da \leq 10^{-2}$), the Hartmann number ($0 \leq Ha \leq 100$), the medium porosity ($0 \leq \varepsilon \leq 1$), the cavity inclination ($0° \leq \varphi \leq 90°$) and the magnetic field orientation ($0° \leq \psi \leq 90°$), defined as:

$$\begin{cases} Ra = \frac{g\beta \Delta T H^3}{\nu \alpha}, \quad \Pr = \frac{\nu}{\alpha}, \\ Da = \frac{\kappa}{H^2} \text{ and } Ha = HB\sqrt{\sigma/\mu} \end{cases} \qquad (3)$$

The convergence criterion for steady state is defined as follows:

$$\left| \frac{\overline{Nu}(t + 5000\Delta t) - \overline{Nu}(t)}{\overline{Nu}(t)} \right| \leq 10^{-4} \qquad (4)$$

2.2 Continuum Formulation and Traditional Solution Methods

The physic of the problem is described as follows: The buoyancy force, acting parallel to the gravity vector, ascends the warm fluid particles which leave the hot wall to replace the cold particles at the upper region, the convective currents push the fluid to circulate near the walls. The movement is enhanced by increasing the temperature gradient, thus, the buoyancy force. Under a magnetic field (Lorentz force), the flow is decelerated and the convective motions are dumped with increasing the magnetic field strength which introduce a control parameter for the convective currents. The flow is governed by the Partial Differential Equations (PDE) that can be solved by using the classical numerical methods in CFD such as Finite Volumes (FV), Finite Elements (FE), Finite Difference (FD) or SPectral (SP) methods or using the new CFD tool, namely the LB method accounting for some considerations that will be shown in details in the following sections.

Under the Boussinesq approximation: $\rho = \rho_0 \left(1 - \beta(T - T_\infty)\right)$, ($T_\infty$ is the reference temperature taken here the cold temperature) the Local Thermal Equilibrium assumption between fluid and solid phases and neglecting viscous heat dissipation and compression work done by the pressure, the averaged governing equations at the REV scale for the generalized model can be summarized for an incompressible fluid as follows:

Continuity

$$\frac{\partial u_i}{\partial x_i} = 0 \tag{5}$$

Momentum

$$\frac{\rho_f}{\varepsilon}\left[\frac{\partial u_i}{\partial t} + \frac{\partial}{\partial x_j}\left(\frac{u_j u_i}{\varepsilon}\right)\right] = -\frac{1}{\varepsilon}\frac{\partial}{\partial x_i}\left(\frac{p}{\varepsilon}\right) + \frac{1}{\varepsilon}\frac{\partial}{\partial x_i}\left(\mu\frac{\partial u_i}{\partial x_i}\right) + \frac{\rho_f}{\varepsilon}F_i \tag{6}$$

Energy

$$\Lambda\left[\frac{\partial T}{\partial t} + u_i\frac{\partial T}{\partial x_i}\right] = \frac{\partial}{\partial x_i}\left(k_e\frac{\partial T}{\partial x_i}\right) \tag{7}$$

$$F_i = -\frac{\varepsilon \, v_e}{\kappa}u_i - \varepsilon F_\varepsilon\sqrt{\frac{u_i u_i}{\kappa}}u_i + \varepsilon g_i\beta(T - T_\infty) \tag{8}$$

Where $g_i \equiv (g\sin(\varphi), g\cos(\varphi))$ are the gravity-field components in the $x - y$ system axis and $\Lambda = \varepsilon(\rho C_p)_f + (1 - \varepsilon)(\rho C_p)_s$.

Where the subscripts f and s correspond to fluid and solid phases and F_i is the forcing term components accounting for the porous medium and the buoyancy effects.

The first and second terms of F_i are the linear (LD) and non-linear (NLD) drags; the last term is the buoyancy force due to the gravity. The effective viscosity v_e is usually taken equal the fluid kinematic viscosity v.

Assuming the ratio between averaged heat capacity and the fluid heat capacity is the unity, the fluid diffusivity α is defined as the ratio between the effective conductivity k_e and the fluid heat capacity $(\rho C_p)_f$.

If the medium characteristics (porosity ε, diameter of the solid particle d_p) are defined, the relationship between the permeability κ and the porosity can be evaluated using the Kozeny-Carman's model as:

$$\kappa = \frac{\varepsilon^3 d_p^2}{36\,\eta\,(1-\varepsilon)^2} \tag{9}$$

Where η is a structural factor that depends on the particles shape and varies in the range $4<\eta<5$ as mentioned in (Alves, Neto et al. (2001). Taking $\eta=4.167$, the relation in Eq. (9) meets the Ergun's experimental model established as:

$$\kappa = \frac{\varepsilon^3 d_p^2}{150\,(1-\varepsilon)^2}, \quad F_\varepsilon = \frac{1.75}{\sqrt{150\,\varepsilon^3}} \tag{10}$$

F_ε is a geometric parameter.

Dividing the non-linear drag (NLD) by linear drag (LD), we found that it can be expressed in term of the viscous diffusion velocity v/H modulated by a factor depending on the porous medium characteristics (ε and Da) as:

$$\frac{|u|F_\varepsilon/\sqrt{\kappa}}{v_e/\kappa} = \frac{|u|}{U_1} \tag{11}$$

where $U_1 = 7\sqrt{\varepsilon^3/Da}.\frac{v}{H}$.

Note that such a formula based on the Ergun's model and can give us idea to simplify Eq. (8).

In the presence of a magnetic field $\boldsymbol{B}$ oriented to an angle ψ from the x-axis, an electromagnetic force $\mathbf{F}_{em}$ (Lorentz force) must be added to the forcing term F_i and is written as:

$$F_{em-i} = \sigma\left[(B_j u_j)B_i - B^2 u_i\right] \tag{12}$$

where σ is the electrical conductivity of the ?uid and B_j denotes the magnetic fields components $B_x = B\,cos(\psi)$ and $B_y = B\,sin(\psi)$. We assume the Joule heating can be neglected since $Ra>10^3$ and $Ha<200$.

In general case, the cavity is inclined from the horizontal in the clockwise direction by an angle ϕ (Fig. 1). The forcing term of Eq. (8), in its two-dimensional final form, will take the following form:

$$F_i = \varepsilon \left(g_i \beta (T_\infty - T) - \frac{v_e}{\kappa} u_i - F_\varepsilon \sqrt{u_i u_i / \kappa} u_i + \sigma \left[(B_j u_j) B_i - B^2 u_i \right] \right) \tag{13}$$

The continuity, momentum and energy equations are solved in the lattice Boltzmann space and scaled by the above mentioned reference scales when presented in the following.

2.3 Solution Based on Lattice Boltzmann Method

In the last decades the LB method is considered to to offer progressively an alternative numerical method traditional Computational Fluid Dynamics (CFD) for simulating fluid flows. In the LBM approach, the fluid is modeled by fictitous particle modeled by distribution functions that occupy nodes and transit to neighboring nodes in a streaming phase. The Poisson equation is time consuming and its solution takes typically 80–90% of the CPU time in traditional CFD solvers (Madabhushi and Vanka (1991)), its absence in LBM means that codes are comparatively fast based on time step per grid point. We have found that a D2Q9-D2Q4 lattice is a suitable model for simulating thermal flows, for the raisons that is more stable then the D2Q9-D2Q9 model, it preserves the computational efforts, since the collision step takes around 70% of the CPU time (Djebali and ElGanaoui (2011)).

The evolution of the distribution functions in the D2Q9-D2Q4 lattice model in the presence of source term S_k is written as follows:

$$\begin{cases} f_k(x',t') - f_k(x,t) = \\ - \left(f_k(x,t) - f_k^{eq}(x,t) \right) / \tau_v + \Delta t\, S_k, \ k = 0,8 \\ g_k(x',t') - g_k(x,t) = \\ - \left(g_k(x,t) - g_k^{eq}(x,t) \right) / \tau_\alpha, \quad k = 1,4 \end{cases} \tag{14}$$

Where $x' = x + e_k \Delta t$, $t' = t + \Delta t$, $\mathbf{x}$ is the lattice site, Δt is the time step, Δx is the lattice grid spacing unit ($=\Delta y=1$), e_k discrete lattice velocity, and f_k and g_k are the density and temperature distribution functions. The correspondent equilibrium parts f_k^{eq} and g_k^{eq} are defined as:

$$\begin{cases} f_k^{eq}(x,t) = \omega_k \rho \left[1 + 3\, e_k.u + 4.5\, (e_k.u)^2 - 1.5\, u^2 \right] \\ g_k^{eq}(x,t) = 0.25\, T\left[1 + 2\, e_k.u \right] \end{cases} \tag{15}$$

It was demonstrated in (Guo, Zheng et al. (2002)) that the suitable form of the forcing term S_k for incompressible fluid flow is written as:

$$S_k = w_k \rho \left(1 - \frac{1}{2\tau_v}\right) \left(\frac{e_k \cdot F}{3} + \frac{uF : (e_k e_k - 3I)}{9\varepsilon}\right) \tag{16}$$

Where $F \equiv F_i$, i=1, 2.

The single-relaxation-times τ_v and τ_α are linked to the kinematic viscosity and the heat diffusivity as

$$v = \frac{2\tau_v - 1}{6} \frac{\Delta x^2}{\Delta t}, \quad \alpha = \frac{2\tau_\alpha - 1}{4} \frac{\Delta x^2}{\Delta t} \tag{17}$$

ω_k are weighting factors and e_k are the lattice velocity vectors. For the D2Q9 LB model we have:

$$\begin{pmatrix} \omega_k \\ e_{k,x} \\ e_{k,y} \end{pmatrix} = \begin{pmatrix} \frac{4}{9}, & \frac{1}{9}, & \frac{1}{9}, & \frac{1}{9}, & \frac{1}{9}, & \frac{1}{36}, & \frac{1}{36}, & \frac{1}{36}, & \frac{1}{36} \\ 0, & 1, & 0, & -1, & 0, & 1, & -1, & -1, & 1 \\ 0, & 0, & 1, & 0, & -1, & 1, & 1, & -1, & -1 \end{pmatrix} \tag{18}$$

It is well to mention that the Prandtl number can be linked to the relaxation times in D2Q9-D2Q4 double population approach as:

$$Pr = \frac{2}{3} \frac{\tau_v - 0.5}{\tau_\alpha - 0.5} \tag{19}$$

In LB heat and flow modeling philosophy, the macroscopic variables: density, velocity and temperature, are computed as follows:

$$\begin{cases} \rho(x,t) = \sum_{k=0,8} f_k & (1) \\ \rho u(x,t) = \sum_{k=0,8} e_k f_k + \frac{\Delta t}{2} F & (2) \\ T = \sum_{k=1,4} g_k & (3) \end{cases} \tag{20}$$

We note that in the velocity field computation, we will not use the same procedure typically adopted in Seta, Takegoshi et al. (2006) and Guo and Zhao (2005); that is to take advantage of the quadratic form of Eq. (20.2) to obtain new formulation. Due the complexity of the complexity of Eq. (20.2) in term of the velocity vector (**u**), in our algorithm, a *new-old* technique is adopted, ie to compute $\mathbf{u}^{new}$ we use $F(\mathbf{u}^{old})$ (in Eqs. (13) and (16)), where $\mathbf{u}^{old}$ and $\mathbf{u}^{new}$ are the velocity fields in two successive iterations t and $t+\Delta t$. Using this technique in spite of that adopted in

Seta, Takegoshi et al. (2006) and Guo and Zhao (2005), will not have effect on the results since the time-step in LB method is very short.

Finally, to accelerate the steady state convergence, the procedure used in (Premnath, Pattison et al. (2009)) is adopted here. That is by incorporating accelerating parameters γ_v and γ_α in Eqs. (15-17):

$$\begin{cases} f_k^{eq}(x,t) = \omega_k \rho [1 + 3\,e_k.u + \frac{4.5\,(e_k.u)^2 - 1.5\,u^2}{\gamma_v}] \\ g_k^{eq}(x,t) = 0.25\,T\,[1 + \frac{2\,e_k.u}{\gamma_\alpha}] \end{cases} \tag{21}$$

and

$$\frac{v}{\gamma_v} = \frac{2\tau_v - 1}{6} \frac{\Delta x^2}{\Delta t}, \qquad \frac{\alpha}{\gamma_\alpha} = \frac{2\tau_\alpha - 1}{4} \frac{\Delta x^2}{\Delta t} \tag{22}$$

More details on the application of this technique in thermal flows can be found in (Djebali and ElGanaoui (2011)). The accelerating parameters γ_v and γ_α are chosen here to be 0.1 for all cases. The kinematic viscosity is taken 0.01, 0.007, 0.003 and 0.002 for Ra of the same order of 10^3-10^4, 10^5, 10^6 and 10^7 respectively.

2.4   Boundary conditions treatments

Implementation of boundaries conditions is a very important issue in LBM since it affects the accuracy of the computations. The second-order bounce back boundary rule for the non-equilibrium distribution function proposed by Zou and He (1997) is used to account for the no-slip boundary condition along the four walls as:

$$(f - f^{eq})^< = (f - f^{eq})^> \tag{23}$$

where the asterisk "<" and ">" denote inner and outer particles respectively at the wall node.

For the temperature field, the temperature distribution functions at the isothermal walls obey:

$$g^< = -g^> + 0.5\,T_{wall} \tag{24}$$

The adiabatic boundary condition is transferred to Dirichlet-type condition using the conventional second-order finite difference approximation as:

$$q_{wall} \approx -k_e \left(\frac{3g_{wall} - 4g_1 + g_2}{2\Delta x} \right) + O(\Delta x^2) \tag{25}$$

3 Results and Analysis

We note that we have validated our thermal LB codes for previously (see the re-
views articles Djebali, Sammouda et al. (2010); ElGanaoui and Djebali (2010) and
Djebali and ElGanaoui (2011))). The present work defines a step ahead to consider
complex situations. Namely the buoyancy-driven flow in air-filled square porous
media with heated differentially walls is here considered. The problem was stud-
ied in parts previously (Nithiarasu, Seetharamu et al. (1997)) using the FE method
and recently (Guo and Zhao (2005)) using the LB method. The authors' results are
gathered to the present ones for comparison sake for different Darcy and Rayleigh
numbers and medium porosities. The second numerical test is a natural-convection
free-fluid flow under a uniform magnetic field; the solution is obtained later by
using the ADI (Alternating Direction Implicit) method. The comparisons are indi-
cated by the averaged Nusselt over the computational domain. The stream-function
and isotherms contours are also plotted and analyzed.

3.1 Test Case 1: Porous Media Flow

By taking ε=1, the Eq. (6) reduces to the standard Navier-Stokes equations for
fluid flow. Our results for Pr=0.71 and Da=10^{10} are compared to those of de Vahl
Davis (1983) and Le Quéré and Roquefort (1985) under the above mentioned lattice
sizes (Table 1). It is found that the present LB thermal model provides satisfactory
agreement. The maximum error observed is less than 1%, which is acceptable for
engineering applications. The divergence at the insulated walls is of $O(10^{-7})$ order
which confirms the second order differencing in Eq. (25).

Table 1: Comparison of the average Nusselt number with de a- de Vahl Davis
(1983) and b- Le Quere, and De Roquefort (1985) for Pr=0.71.

	Ra	10^3	10^4	10^5	10^6	10^7
	a	1.118	2.243	4.519	8.800	-
$\overline{Nu}$	b	1.118	2.245	4.522	8.825	16.520
	Present	1.116	2.229	4.484	8.734	16.376

The grid sensitivity is also tested to let our code giving accurate predictions. Table
2 shows that the above mentioned grid sizes are the appropriate for the correspond-
ing Rayleigh numbers. Cite for example for Ra=10^5, the Nusselt number change
amount is about 0.09% from the grid size 90×90 to 100×100.

In this test we set ε=0.4, Pr=1, the Rayleigh number varies from 10^3 to 10^7 and the
Darcy parameter takes 10^{-4} and 10^{-2}. In the computations, we use the lattice sizes
ranging from 50 to 150 by step 25 when increasing the Rayleigh numbers from 10^3

Table 2: Grid sensitivity check based on the average Nusselt number $\overline{Nu}$ for Pr=0.71.

Grid size		50×50	60×60	70×70	80×80	90×90	100×100
Ra=	10^4	2.2204	2.2245	2.2273	2.2294		
	10^5			4.4670	4.4746	4.4802	4.4841
Grid size		100×100	110×110	120×120	130×130	140×140	150×150
Ra=	10^6	8.7044	8.7183	8.7343	8.7348		
	10^7				16.3475	16.3662	16.3764

Table 3: Comparison of the average Nusselt number with c- Guo and Zhao (2005) and d- Nithiarasu, Seetharamu et al. (1997) for Pr=1

Da	Ra	$\varepsilon=0.4$				$\varepsilon=0.6$	
		Present	c	d		Present	d
10^{-4}	10^5	1.066	1.066	1.067		1.072	1.071
	10^6	2.595	2.603	2.550		2.711	2.725
	10^7	7.816	7.788	7.810		8.532	8.183
10^{-2}	10^3	1.008	1.008	1.010		1.013	1.015
	10^4	1.360	1.367	1.408		1.491	1.530
	10^5	2.989	2.988	2.983		3.435	3.555

Table 4: Comparison of the average Nusselt number $\overline{Nu}_0$ obtained using the LBM with ADI predictions (Rudraiah, Barron et al. (1995)) for Pr=0.733, symbol "†" denotes our results.

Ra/Pr	Ha=10			Ha=50			Ha=100		
	LBM[†]	FVM[†]	ADI	LBM[†]	FVM[†]	ADI	LBM[†]	FVM[†]	ADI
2.10⁴	2.2780	2.2976	2.2234	1.0900	1.1154	1.0856	1.0177	1.0113	1.0110
2.10⁵	5.0518	4.9865	4.8053	3.0784	3.2901	2.8442	1.4866	1.6430	1.4317
2.10⁶	9.8852	9,7904	8.6463	8.9326	9.0563	7.5825	6.7142	7.2416	5.5415

to 10^7(respectively). Figure 2 presents the streamline contours and the isotherm lines for *Da*=10^{-4} and a Rayleigh number ranging from 10^5 to 10^7. It is well observed, qualitatively, that our results agree well with the previous findings. When increasing the Rayleigh number, the flow patterns show an inclined stratification for the temperature fields and the boundary layers become more stretched to the isothermal walls. Quantitatively, the averaged Nusselt number is tabulated in Table 3 for different *Da* and *Ra*. The present predicted results are gathered to available referenced results based on different numerical methods.
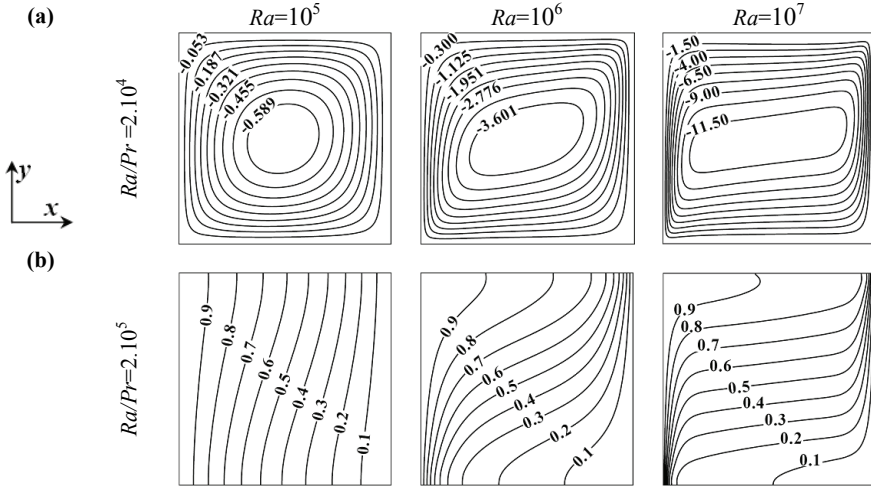
Figure 2: Dynamic (a) and thermal (b) structures for $\varepsilon=0.4$, $Pr=1$, $Da=10^{-4}$.

In modeling porous media flows, it is important to know the ratio NLD/LD, which determines the limit of using the two above mentioned models for porous media flows. In convection flows, the characteristic velocity is $U_0 = \sqrt{g\beta\Delta TH}$, the ratio NLD/LD as defined in Eq. (11) expressed as function of flow , medium and fluid parameters reads:

$$\frac{NLD}{LD} = \frac{1}{7}\sqrt{\frac{Ra}{Pr}\frac{Da}{\varepsilon^3}} \tag{26}$$

A computation is performed for $Ra=10^4$, $Da=10^{-4}$, Pr=1 and $\varepsilon=0.9$, leading to NLD/LD=0.196. It has been shown that the present generalized model with and without NLD term (ie setting $F_\varepsilon=0$ in Eq. (8)) does not show significant difference.

3.2 Test Case 2: Free-fluid Flow under Vertical Magnetic Field

The following section consists of simulating free fluid flow in a square cavity heated and cooled on side walls and insulated on the horizontal walls, previously investigated by Rudraiah, Barron et al. (1995). The fluid flow is subjected to the effects of buoyancy and a vertical (descendent) magnetic field. The heat transfer is quantified by the averaged Nusselt number $\overline{Nu}_0$ along the hot wall for a wide range of parameters ($14660 \leq Ra \leq 1466000$, $0 \leq Ha \leq 100$, $Pr=0.733$). The present numerical solutions are summarized in Table 4 and compared to Rudraiah's results using the ADI (Alternating Direction Implicit) method. To check the justness of our results

for the average Nusselt number, a test is made using the Finite Volume method. We have remarked that the present LB results agree well with those of the FVM ones. Our codes give also patterns of the streamlines and isotherms very similar to the Ece and Büyük (2006)'s results. However their numerical results are found to be under estimated by unity.

The force-ratio of the buoyancy to the electromagnetic ones is proportional to Ra/Ha^2. It is well known that the Lorentz force reduces velocities and dumps the convection currents and heat transfer. Accordingly, major effects are observed between the cases: with/without Lorentz force. In the studied ranges of the monitoring number, the buoyancy force is more effective as $Ra > 10^4$ (since $Ra/Ha^2 \gg 1$), the rise of the Nusselt number is more expressed as shown in Tab. 3. See for example for $Ha=100$, the Nusselt number rise from $Ra=14660$ to 146600 is about 46% and it is about 352% from $Ra=146600$ to 1466000 since magnetic force dumps convective current then heat transfer, but it has minor effects for high Rayleigh numbers since $Ra/Ha^2 \gg 1$.

Figures 3(a) and 3(b) show the streamlines and isotherms contours for different inclination angles for both the cavity and the magnetic field at $Ra=10^5$. The magnetic force is expressed as $F_{em} = -\sigma B^2 u_x$, then it opposes to the convective currents. We see for example, for $Ha=10$ a thermal stratification is well established by increasing the Rayleigh number to 1466000. However, increasing the Hartmann number to 100, the isotherms contours undergo a counter-clockwise rotation, meaning that only a vertical flowing is allowed.

3.3   *Porous Media Flow under Magnetic Field*

In this section the combined effect of porous medium and external magnetic force on flow pattern is considered. A parametric study exploring the parameters effects is proposed based on three axes: first, the effect of the Rayleigh number (10^4 to 10^6) and the cavity inclination ($0°$ to $90°$), second, the effect of the Darcy number (10^{-4} to 10^{-2}) and the medium porosity (0.4 to 0.8), and last, the effect of the Hartmann number (10 to 100) and the magnetic field inclination ($0°$ to $90°$). The Prandtl number is chosen to be 1.

The numerical simulations are carried out based on the same conditions presented in section 2.4.

Rayleigh Number and Cavity Inclination Effects: To account for this combined effect in the porous medium in the presence magnetic field, we set $\varepsilon=0.4$, $Da=10^{-2}$, $Ha=50$ and $\psi=0°$. As shown in Figs. 4(a) and 4(b), variations of the Rayleigh number and the cavity inclination have important effects on dynamic and thermal fields structures. For $\phi=0°$, increasing the buoyancy force (Ra) enhances the convective
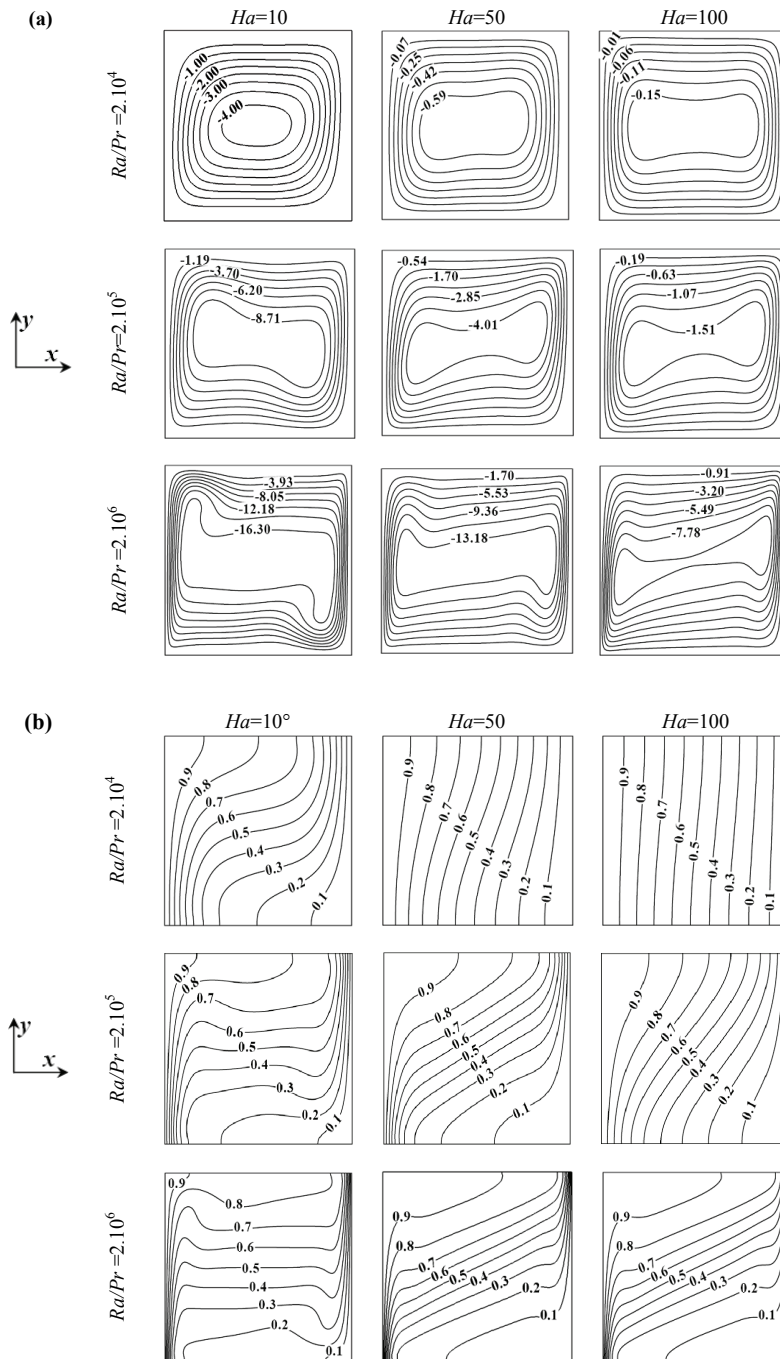
Figure 3: Dynamic (a) and thermal (b) structures for free fluid flow for *Pr*=0.733 and *ϕ*=0°
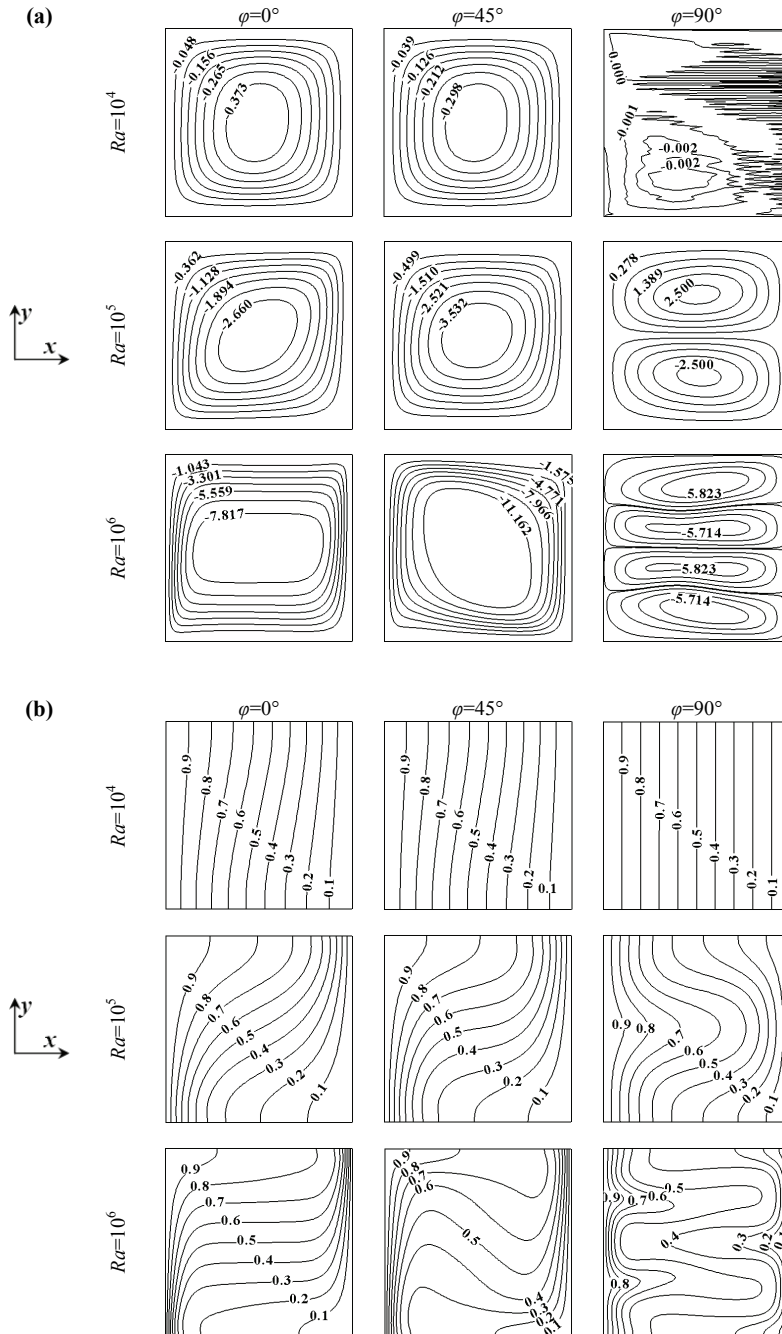
Figure 4: Dynamic (a) and thermal (b) structures for Pr=1, Da=10^{-2}, ε=0.4, Ha=50, and ψ=0˚.

currents dumped (or suppressed) by the magnetic force effect for low Rayleigh numbers. The isotherms become stretched near the isothermal walls and equally spaced at the cavity core leading to a fully established stratification. For high cavity inclination (ϕ=90˚) in the counter-clockwise direction, the flow pattern is more complex due to the Rayleigh-Bénard phenomenon: the heat transfer is purely conductive for Ra=10^4 and a pair and two-pair-counter-rotating cells are formed for (respectively) Ra=10^5 and 10^6, compared to free fluid flow in enclosure.

The flow pattern is more illustrated when plotting the velocity components at mid-height and mid-width (Fig. 5). With increasing the Rayleigh number, the x-velocity magnitude increases and its maximums locations displace to the horizontal adiabatic walls. The same behaviour is presented for the y-velocity with a maximum location moving near the isotherm walls. similarly, increasing the inclination angle reduces the velocity components for lowers Rayleigh numbers (due to the conductive regime) but raises the velocity components for high Rayleigh number (due to the Rayleigh-Bénard convection). The averaged Nusselt number at the isothermal wall for Ra=10^6 is 5.0647, 5.4169 and 4.3969 for respectively ϕ=0˚, 45˚ and 90˚.

Darcy Number and Medium Porosity Effects: In this part we choose Ra=10^5, Ha=50 and ϕ= ψ =0˚.The flow structure is for all a single clockwise rotating cell. As for the previous investigation, the effects of the Darcy number and the medium porosity are significant. With decreasing the Darcy number (logarithmically), the infiltration velocity in the medium decreases considerably, the thermal behavior tends to take a conductive mode signature.

The presence of the magnetic field results in decreasing the heat transfer compared to the case of flow in porous media without external force and forming in somewhat a diagonal-acting region as shown in Figs. 7(a) and 7(b). On the other hand, increasing the medium porosity enhances slightly the convective currents near the insulated walls, resulting in a small rotation of the isotherms and diagonally-extending the elliptic cell at the core.

In general, for the chosen dimensionless parameters there are no significant changes in the flow and thermal behaviors when varying the medium porosity under the present magnetic field magnitude. The change should be more expressed for low Hartmann number, since increasing the medium porosity results in a free fluid flow.

As we can see, also, in Fig. 6, the flow presents a symmetric pattern relative to the cavity center. For a fixed Darcy number, increasing the medium porosity raises the maximum value of u(0.5,y) and v(x,0.5).

However, increasing the Darcy number reduces effectively the velocity components strength: as for ε=0.8, the x-velocity and its y-location are 13.5501(0.91),
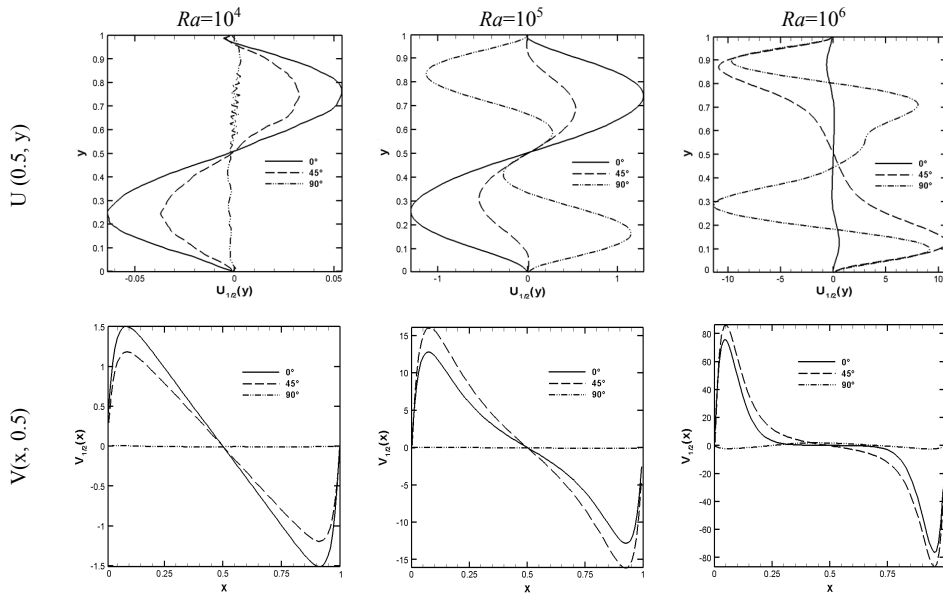
Figure 5: Velocities profiles at the horizontal and vertical mid-plans for different Rayleigh numbers and cavity inclinations for $Da=10^{-2}$, $\varepsilon=0.4$, and $Ha=50$.
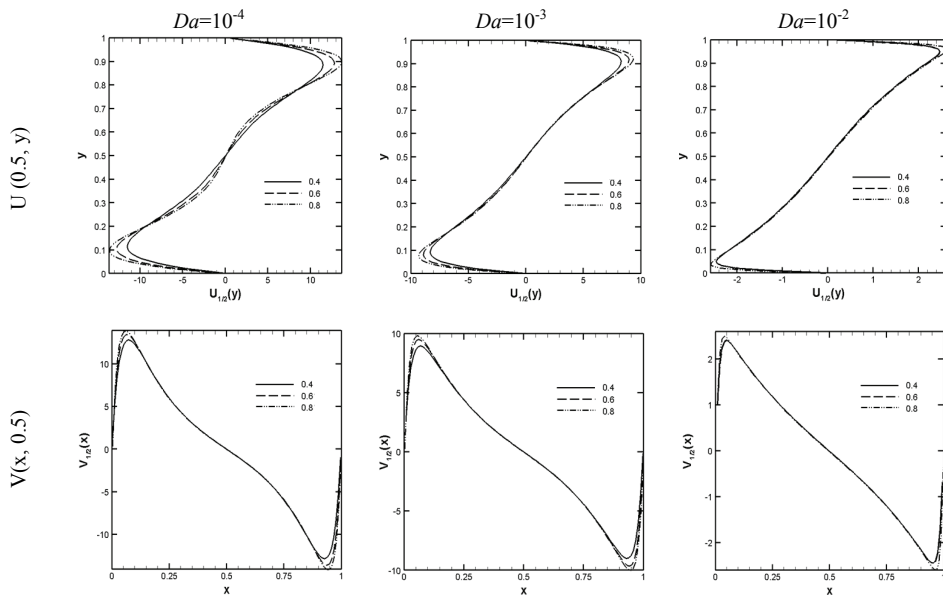
Figure 6: Velocities profiles at the horizontal and vertical mid-plans for different Darcy numbers and medium porosities for $Ra=10^5$, $\varphi=0°$, and $Ha=50$.
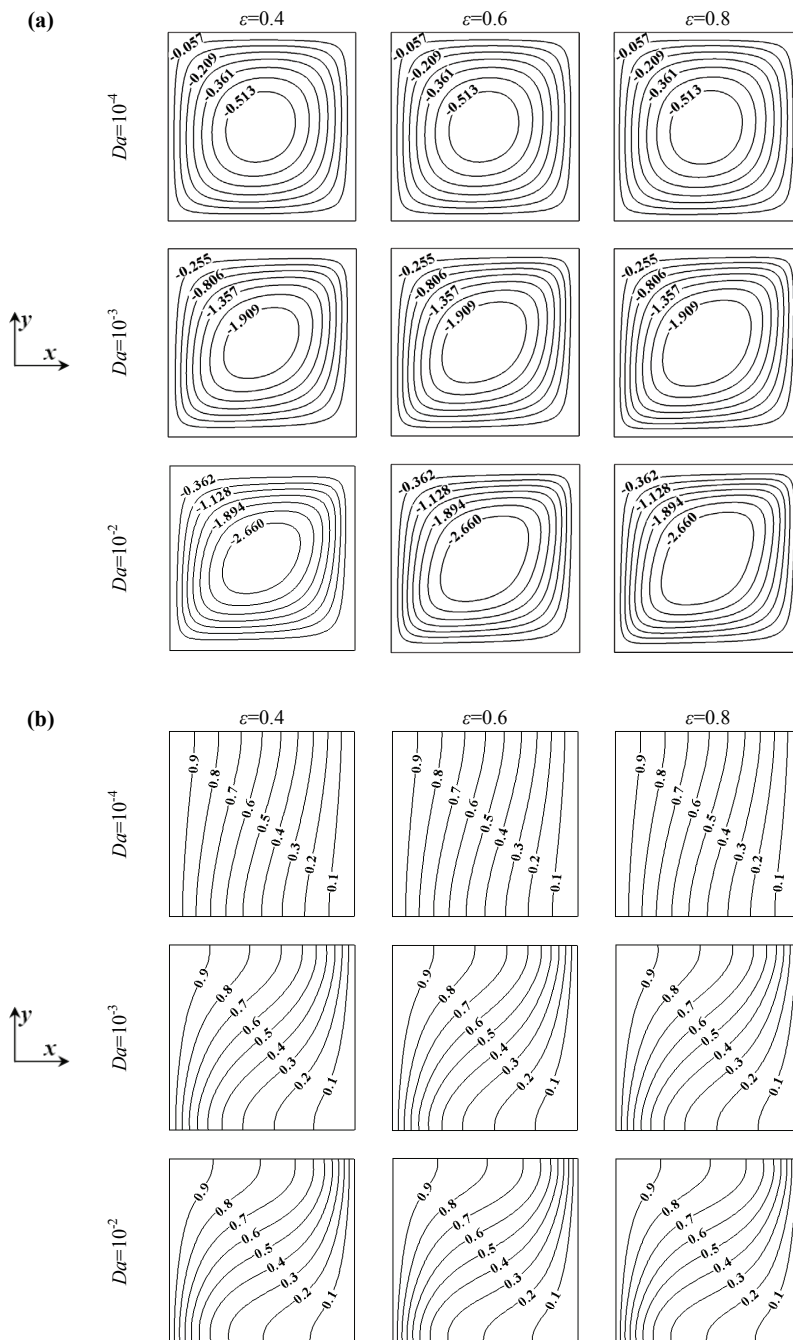
Figure 7: Dynamic (a) and thermal (b) structures for $Ra=10^5$, $\phi=0°$, $Pr=1$, $Ha=50$ and $\psi=0°$.
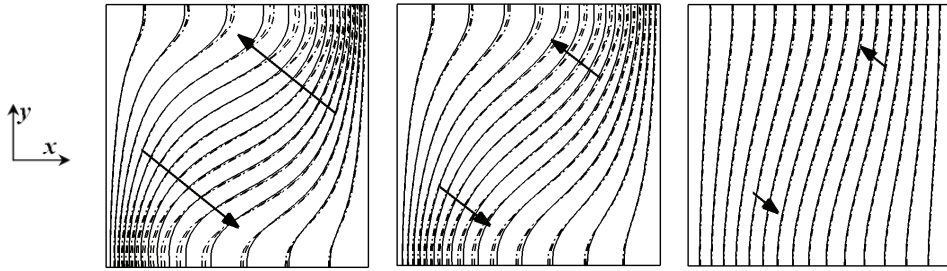
Figure 8: Effect of the Darcy number on thermal structure for $Da=10^{-4}$, 10^{-3} and 10^{-2} (from left to right). For $Ra=10^5$, $\phi=0°$, $Pr=1$, $Ha=50$ and $\psi=0°$. $\varepsilon=0.4$: solid line, $\varepsilon=0.6$: dashed line and $\varepsilon=0.8$: dash-doted line.
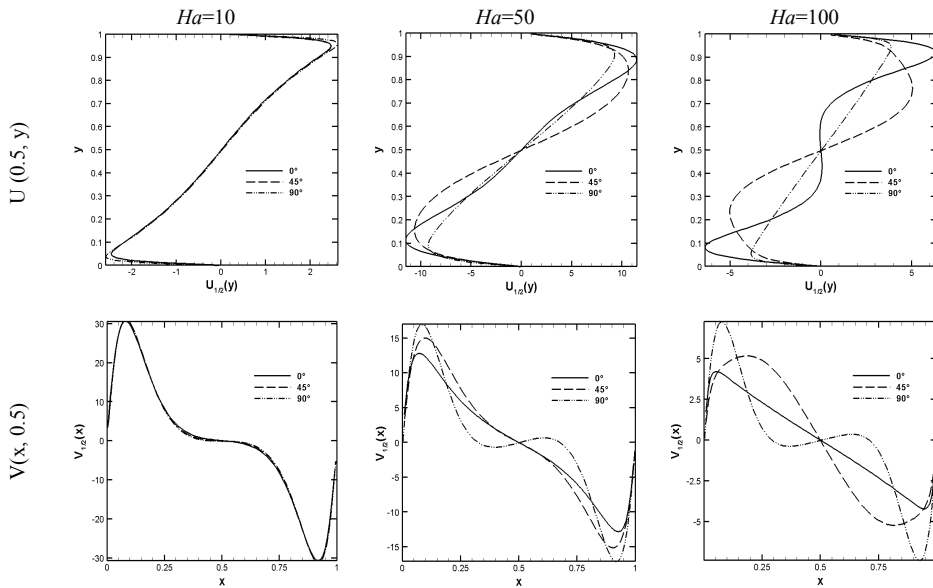
Figure 9: Velocities profiles at the horizontal and vertical mid-plans for different Hartmann numbers and magnetic field orientations for $Ra=10^5$, $\varphi=0°$, $Da=10^{-2}$ and $\varepsilon=0.4$.

9.2687(0.93) and 2.6161(0.97) for respectively $Da= 10^{-4}$, 10^{-3} and 10^{-2}. Then, their location moves gradually towards the wall. The behaviour is the same for the y-velocity component: the y-velocity and its x-location are: 13.9512(0.08), 9.9380(0.06) and 2.5143(0.05) for $Da=10^{-4}$, 10^{-3} and 10^{-2} respectively. More-
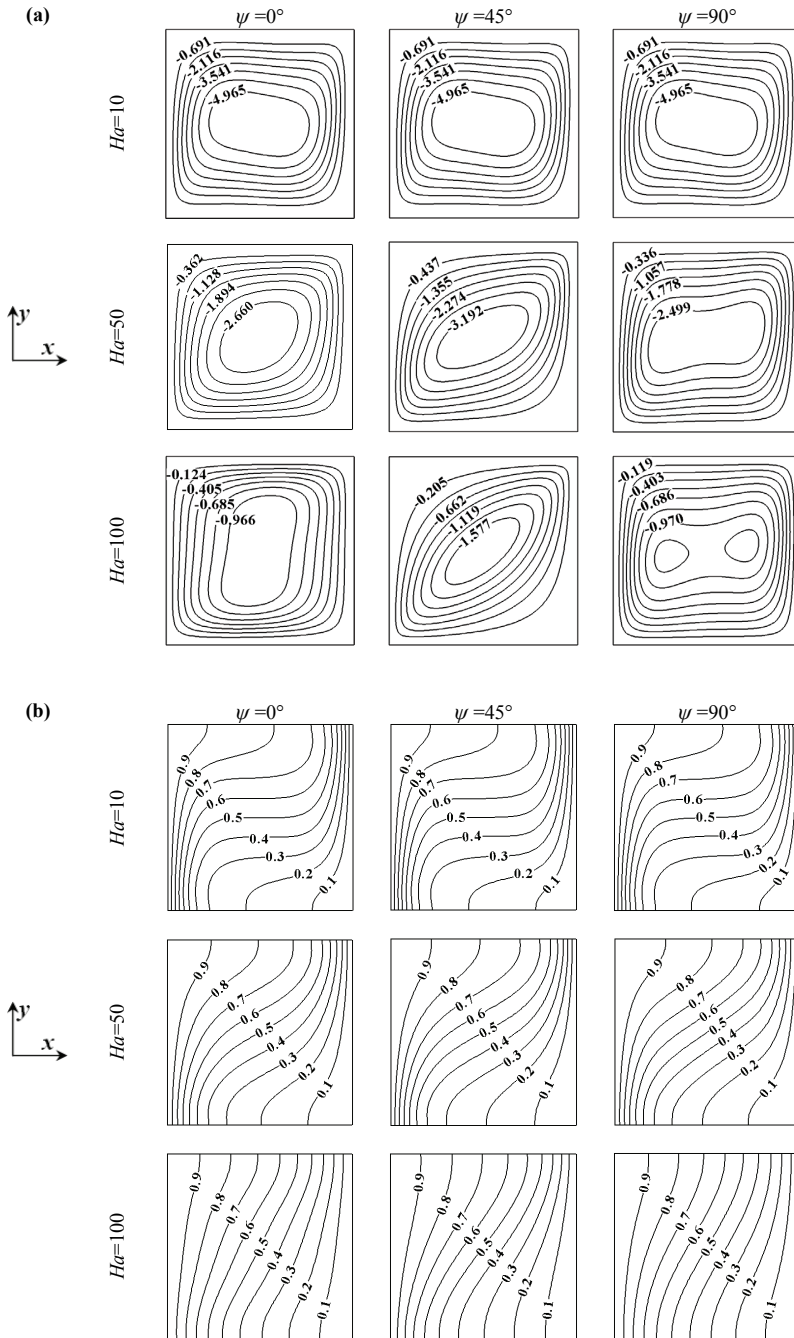
Figure 10: Dynamic (a) and thermal (b) structures for $Ra=10^5$, $\phi=0°$, $Pr=1$, $Da=10^{-2}$ and $\varepsilon=0.4$

over, the porosity effect is found to be suppressed with increasing Darcy number: for low Darcy number, the medium porosity has a modest effect, but has little effect for high Darcy number. This behaviour is well demonstrated in Fig. 8, that by decreasing the medium porosity, the thermal structure undergoes a counterclockwise rotation. At the same time, increasing the Darcy number, the porosity effect becomes minority.

The averaged Nusselt number at the isothermal wall for $Da=10^{-2}$ is 1.8854, 1.9742 and 2.0305 for respectively $\varepsilon=0.4$, 0.6 and 0.8.

Hartmann Number and Magnetic Field Inclination Effects: In this part we choose $Ra=10^5$, $\phi=0°$, $Da=10^{-2}$ and $\varepsilon=0.4$. As it can be seen in Fig. 9, the inclination angle variation (of the magnetic field) has no effects on mid-plan velocity traces for low Hartmann number ($Ha<10$); the behaviour joins those presented in Fig. 6 ($Da=10^{-2}$). However, for high Hartmann numbers, increasing the angle ψ, there will be a balance between the suppressed rate in the x-velocity and recompensed part in the y-component, that is due to the duality $sin(\psi)$-$cos(\psi)$. For $Ha=100$, the Nusselt number at isothermal walls is 1.2069, 1.3088 and 1.2096 for respectively $\psi=0°$, 45° and 90°.

In Fig. 10(a) and 10(b), one can say that the magnetic field strength and inclination have the significant effect on the dynamic structure. The thermal structure seems to be indifferent to the magnetic field inclination. This is confirmed by the quasi constant heat transfer for the three Hartmann number values. The relative Nusselt number variation is less than 3%, obtained for $Ha=50$. When the magnetic field is applied in 'x+' direction the central eddy is extended in the vertical direction and slows down with increasing the Hartman number. When the magnetic field is applied diagonally, the dynamic structure becomes more extended diagonally. When the magnetic field is applied in the 'y+' direction the dynamic central eddy becomes extended horizontally and two small vortices appear in the core region. Increasing more the Hartmann number, the isotherms becomes equally spaced yielding to a diagonal thermal stratification.

4   Conclusion

Several numerical simulations have been conducted in the past by using conventional numerical method based on discretization of macroscopic equations. Dealing with transfers in complex media, mostly, numerical studies in CFD suffer from many difficulties, such as stability, accuracy, computational cost, memory requirements...

Recently, the Lattice Boltzmann Method (LBM) has met with significant success for numerical simulation and modeling of many classical and complex flows. In

recent works of the authors, investigations shown the validity and the accuracy for the based LBM classes of methods for solving flow dynamic, and extended development to thermal LBM provided results for coupled heat and dynamic fields noticeably involving solid/liquid transition.

LB method is found to be more practical at least for saving computational time and easy incorporating source terms, like for this study investigating heat and fluid flow under buoyancy and external inclined magnetic forces.

This paper provides a step ahead on the validation and confirmation of potential use of the LBM class of methods for stiff applications.

Two degrees of complex conditions has been considered in the present paper to fully investigating the dynamic and thermal behavior in porous medium, flow under uniform magnetic field and their combination in a square enclosure.

The flow and thermal patterns depend strongly on the Rayleigh number the Darcy parameter and the cavity inclination, however it depend marginally on the medium porosity under moderate Hartmann number. Increasing the Hartmann number results in suppressing the convective currents inside the cavity and then reducing greatly the heat transfer rate quantified by the help of Nusselt number along heated/-cooled wall and overall the medium. The magnetic field inclination affects strongly the dynamic structure; however, no significant effects for the temperature field have been remarked.

Its is found through this study, that the LB method is a reliable tool for investigating MHD convective heat transfer in confined space. Additionally, this computational technique is so simple for coding, treating boundary conditions, accounting for complex physics such as external magnetic force and porous matrix, and particularly preserving computational cost.

References

Amahmid, A; Hasnaoui, M.; Mamou M. and Vasseur, P. (1999): Double-diffusive parallel flow induced in a horizontal Brinkman porous layer subjected to constant heat and mass fluxes: analytical and numerical studies, *Heat and Mass Transfer*, vol. 35, pp. 409-421.

Arab, M.R.; Semma, E.; Pateyron, B. and El Ganaoui, M. (2009): Determination of physical properties of porous materials by a lattice Boltzmann approach, *FDMP: Fluid Dynamics & Materials Processing*, vol. 5, no. 2, pp. 161-176.

Basak, T.; Roy, S.; Paul, T. and Pop, I. (2006): Natural convection in a square cavity filled with a porous medium: Effects of various thermal boundary conditions, *International Journal of Heat and Mass Transfer*, vol. 49, no. 7-8, pp. 1430-1441.

Chai, Z.; Guo, Z. and B. Shi (2007): Lattice Boltzmann simulation of mixed convection in a driven cavity packed with porous medium, *ICCS, Part I, LNCS* 4487, pp. 802-809.

Chatterjee, D. and Amiroudine, S. (2011): Lattice Boltzmann simulation of thermofluidic transport phenomena in a DC magnetohydrodynamic (MHD) micropump, *Biomed Microdevices*, vol.13, no. 1, pp. 147–157.

Chen, S. and Doolen, G. D. (1998): Lattice Boltzmann method for fluid flows, *Annual Review Fluid Mechanics*, vol. 30, pp. 329-364.

De B. Alves, L.S.; Neto, H.-L. and Cotta, R.M. (2001): Parametric analysis of the stream function time derivative in the Darcy-flow model for transient natural convection. *In Proceedings of the 2nd International Conference on Computational Heat and Mass Transfer,* Brazil, pp. 22-26.

de Vahl Davis G. (1983): Natural convection of air in a square cavity: A benchmark numerical solutions, *International Journal of Numerical Methods Fluids*, vol. 3, pp. 249-264.

Djebali, R. and El Ganaoui, M. (2011): Assessment and computational improvement of thermal lattice Boltzmann models based benchmark computations, *CMES: Computer Modeling in Engineering & Sciences*, vol. 71, no. 3, pp. 179-202.

Djebali, R.; Sammouda, H. and ElGanaoui M. (2010): Some advances in applications of lattice Boltzmann method for complex thermal flows, *Advances in Applied Mathematics and Mechanics*, vol. 2, no. 5, pp. 587-608.

Ece, M.C. and Büyük E. (2006): Natural-convection flow under a magnetic field in an inclined rectangular enclosure heated and cooled on adjacent walls, *Fluid Dynamics Research*, 38, pp. 564-590.

El Ganaoui, M. and Djebali R. (2010); Aptitude of a lattice Boltzmann method for evaluating transitional thresholds for low Prandtl number flows in enclosures, *Compte Rendu Mecanique*, vol. 338, no. 2, pp. 85-96.

Gelfgat, A. Y. and Bar-Yoseph P.-Z. (2001): The effect of an external magnetic field on oscillatory instability of convective flows in a rectangular cavity, *Physic of Fluids*, vol. 13, no. 8, pp. 2269-2278.

Grosan, T.; Revnic, C.; Pop I.and Ingham D.B. (2009): Magnetic field and inter-

nal heat generation effects on the free convection in a rectangular cavity filled with a porous medium, *International Journal of Heat and Mass Transfer*, vol. 52, no. 5-6, pp. 1525-1533.

Guo, Z.; Zheng, C. and Shi, B. (2002): Discrete lattice effects on the forcing term in the lattice Boltzmann method, *Physical Review E,* 65, 046308-1.

Guo, Z. and Zhao, T. S. (2002): Lattice Boltzmann model for incompressible flows through porous media, *Physical Review E*, 66, 036304-1.

Guo, Z. and Zhao, T.S. (2005): A lattice Boltzmann model for convection heat transfer in porous media, *Numerical Heat Transfer*, Part B, 47, pp. 157-177.

Hadavand, M. and Sousa, A.C.M. (2011): Simulation of thermomagnetic convection in a cavity using the lattice Boltzmann model, *Journal of Applied Mathematics*, vol. 2011, Article ID 538637, 14 pages; doi:10.1155/2011/538637.

Hamimid, S.; Guellal, M.; Amroune, A. and Zeraibi, N. (2011): Effect of a porous layer on the fflow structure and heat transfer in a square cavity, *FDMP: Fluid Dynamics & Materials Processing*, vol.8, no.1, pp.69-90.

Hao, L.; Xinhua, L. and Yongzhi, L. (2011): The lattice Boltzmann simulation of magnetic fluid, *Procedia Engineering* , vol. 15, pp.3948-3953.

Hossain, M.A. and Wilson, M. (2002): Natural convection flow in a fluid-saturated porous medium enclosed by non-isothermal walls with heat generation, *International Journal of Thermal Sciences*, vol. 41, no.5, pp. 447-454.

Ingham, D. B. and I. Pop (2005 Eds.), *Transport Phenomena in Porous Media*, Elsevier, Oxford.

Jiang, P.X. and Ren, Z.P. (2001): Numerical investigation of forced convection heat transfer in porous media using a thermal non-equilibrium model, *International Journal of Heat and Fluid Flow*, vol. 22, no.1, pp. 102-110.

Jina, L. and Zhang, X.-R. (2012): Analysis of temperature-sensitive magnetic fluids in a porous square cavity depending on different porosity and Darcy number, *Applied Thermal Engineering*, DOI: 10.1016/j.applthermaleng.2012.05.016.

Le Quéré, P. and De Roquefort, T.A. (1985): Computation of natural convection in two dimensional cavity with Chebyshev polynomials, *Journal of Computational Physics*, vol. 57, no.2, pp. 210-228.

Madabhushi, R.K. and Vanka S.P. (1991): Large eddy simulation of turbulence-driven secondary flow in a square duct, *Physic of Fluids A* , vol. 3, pp. 2734-2745.

Mezrhab, A.; Jami, M.; Bouzidi M. and Lallemand, P. (2007): Analysis of radiation-natural convection in a divided enclosure using the lattice Boltzmann method, *Computers and fluids*, vol. 36, no.2, pp. 423-434.

Nield, D.A. and Bejan, A. (2006): *Convection in porous media*, Third ed. Springer, New York.

Nithiarasu, P.; Seetharamu K. N. and Sundararajan, T. (1997): Natural convective heat transfer in a fluid saturated variable porosity medium, *International Journal of Heat Mass Transfer*, vol. 40, no. 16, pp. 3955-3967.

Pop, I. and Ingham, D.B. (2001): *Convective heat transfer: mathematical and computational modelling of viscous fluids and porous media*, Pergamon, Oxford.

Premnath, K.N.; Pattison, M.J. and Banerjee, S. (2009): Steady state convergence acceleration of the generalized lattice Boltzmann equation with forcing term through preconditioning, *Journal of Computational Physics*, vol. 228, no. 3, pp. 746-769.

Roussellet, V.; Niu, X.; Yamaguchi, H. and Magoulés, F. (2011): Natural convection of temperature-sensitive magnetic fluids in porous media, *Advances in Applied Mathematics and Mechanics,* vol. 3, no. 1, pp. 121-130.

Rudraiah, N.; Barron, R. M.; Venkatachalappa, M. and Subbaray, C.K. (1995): Effect of a magnetic field on free convection in a rectangular enclosure, *International Journal of Engineering Sciences*, vol. 33, no. 8, pp. 1075-1084.

Semma, E.; El Ganaoui, M. ; Bennacer, R.; Mohamad, A. A. (2008): Investigation of flows in solidification by using the lattice Boltzmann method, *International Journal of Thermal Sciences*, vol. 47, no. 3, pp. 201-208.

Seta, T.; Takegoshi, E. and K. Okui (2006): Lattice Boltzmann simulation of natural convection in porous media, *Mathematics and Computers in Simulation*, vol. 72, no. 2-6, pp. 195–200.

Srivastava, N. and Singh A.-K. (2010): Mixed convection in a composite system bounded by vertical walls, *Journal of Applied Fluid Mechanics*, vol. 3, no. 2, pp. 65-75.

Succi, S. (2001): *The lattice Boltzmann equation for fluid dynamics and beyond*, Oxford University Press.

Vafai, K. (2005), *Handbook of porous media*, Second ed. Taylor & Francis, Boca Raton.

Vafai, K. and Tien C.L. (1981): Boundary and inertia effects on flow and heat transfer in porous media, *International Journal of Heat Mass Transfer*, vol. 24, no. 2, pp. 195-203.

Zhang, X.-R.; Jin, L.-C.; Niu, X.-D. and Yamaguchi, H. (2010): Lattice Boltzmann simulation for magnetic fluids in porous medium, *Physics Procedia*, vol. 9, pp. 162-166.

Zou, Q. and He, X. (1997): On pressure and velocity boundary conditions for the

lattice Boltzmann BGK model, *Physics of Fluids*, vol. 9, no. 6, pp. 1591-1598.